

# On the gravitational stratification of multi-fluid-multi-species plasma

F. Zhang<sup>1,2</sup>, J. Martínez-Sykora<sup>3,4,1,2</sup>, Q. M. Wargnier<sup>5</sup>, and V. H. Hansteen<sup>1,2,3</sup>

<sup>1</sup> Institute of Theoretical Astrophysics, University of Oslo, PO Box 1029 Blindern, 0315 Oslo, Norway  
 e-mail: fan.zhang@astro.uio.no

<sup>2</sup> Nansen Center for Solar Physics, University of Oslo, PO Box 1029 Blindern, 0315 Oslo, Norway

<sup>3</sup> SETI Institute, 339 Bernardo Ave, Mountain View, CA 94035, USA

<sup>4</sup> Lockheed Martin Solar and Astrophysics Laboratory, 3251 Hanover St, Palo Alto, CA 94304, USA

<sup>5</sup> Green 14 AB, Brinellvägen 25, Stockholm, Sweden

January 12, 2026

## ABSTRACT

**Context.** The solar atmosphere is gravitationally stratified and consists of several layers at temperatures different by orders of magnitude. Consequently, the solar atmospheric plasma changes from weakly ionized in the photosphere, partially ionized in the chromosphere, to eventually fully ionized in the corona. However, it is still not trivial to integrate ionization and recombination processes into multi-fluid solar plasma models with gravitational stratification.

**Aims.** We intend to provide a method for constructing multi-fluid-multi-species gravitational stratification that satisfies ionization equilibrium and hydrostatic equilibrium at the same time, avoiding causing non-physical disturbances and numerical instability due to initial in-equilibria.

**Methods.** We assume that collisional interactions between fluids are sufficient for coupling all fluids when there is no high-frequency external driving force imposed. Ionization fractions can be (I) calculated assuming ionization in statistical equilibrium at any given temperature, or (II) extracted from other atmospheric models. A simple numerical integration routine is then designed and used to construct multi-fluid-multi-species gravitational stratifications.

**Results.** A gravitational stratification constructed using the present numerical integration routine can be in hydrostatic equilibrium with any given ionization fractions of multi-species plasmas. Meanwhile, without any dynamic driving force, fluid decoupling appears in the transition region of the constructed stratification, while the total velocity of all fluids remains zero.

**Conclusions.** A gravitational stratification constructed using the present routine can be used in multi-fluid-multi-species models to study specific dynamics without being affected by initial in-equilibria.

**Key words.** magnetohydrodynamics – partial ionization – multi-fluid-multi-species – Sun: atmosphere

## 1. Introduction

The solar and stellar atmospheres are highly complex and dynamic. To numerically model and analyze the atmospheres, however, we typically need to make various assumptions and then simplifications. Among them, an important and frequently used one is assuming a 1D "background" or "initial" atmosphere in a static gravitational stratification, following

$$\frac{dP}{dz} = -\varrho g, \quad (1)$$

where total pressure includes thermal pressure of gas plasma and magnetic pressure, i.e.,  $P = p^{\text{g(as)}} + p^{\text{m(agnetic)}}$ ,  $\varrho$  is plasma density,  $g$  is gravitational acceleration, and  $z$  is height. This balance between the total pressure gradient and gravity is assumed to be valid in the atmospheric model in the  $z$ -direction. Note that, in the solar atmosphere the mean free path of particles is much smaller than the characteristic length scales of interest. Therefore, the plasma can be assumed to be close to Maxwellian equilibrium, and a fluid description, e.g. magnetohydrodynamics (MHD), is appropriate. Therefore, the stationary momentum equation reduces to the hydrostatic balance as written in Eq. (1). Models with this assumption have been extensively used to investigate, for example, MHD waves in the solar atmosphere, be-

ing able to provide important insights (Khomenko & Collados 2015; Van Doorsselaere et al. 2020).

However, this common practice encounters challenges when considering multi-fluid (two or more fluids) MHD modeling of, e.g., the low solar atmosphere, where the thermodynamic conditions do not permit a single-fluid description, and instead require a set of coupled governing equations for the ionized and neutral components, commonly referred to as multi-fluid MHD equations (Khomenko 2016; Ballester et al. 2018). While the gravitational acceleration is the same for all fluids, the balance between pressure gradient and density is typically assumed to be independent for each fluid. More specifically, when constructing an initial static atmospheric model, it is frequently assumed that each of the  $n$  fluids is in an independent hydrostatic equilibrium

$$\frac{dP_i}{dz} = -\varrho_i g, \quad i = 1, \dots, n, \quad (2)$$

in which the thermal pressure  $p_i^{\text{g}}$  of the  $i$ -th fluid includes the thermal pressure of the free electrons produced when the  $i$ -th fluid undergoes ionization. For example, in various pure-hydrogen ion-neutral two-fluid models (Alvarez Laguna et al. 2016; Popescu Braileanu et al. 2019; Wójcik et al. 2020; Popescu Braileanu & Keppens 2023), the equations of state of

neutral and ionized hydrogen are, respectively,

$$p_{n(\text{neutral})}^g = N_n k_B T_n, \quad (3)$$

and

$$p_{i(\text{ion})}^g = N_i k_B T_i + N_{e(\text{electron})} k_B T_e = 2N_i k_B T_i, \quad (4)$$

where  $N$  and  $T$  denote the number densities and temperatures, with subscripts  $i$ ,  $n$ , and  $e$  indicating ionized hydrogen, neutral hydrogen, and free electrons, respectively;  $k_B$  is the Boltzmann constant. In these models, the description of free electrons is simplified, ignoring the thermal force, which is feasible for modeling the low solar atmosphere which can be assumed to be nearly isothermal (Hansteen et al. 1997). In addition, Eq. (4) assumes that the ion temperature and electron temperature are the same. This assumption simplifies the numerical model but is not a necessary constraint for the solar atmosphere.

Directly using Eq. (2) to calculate a multi-fluid gravitational stratification causes practical issues. Essentially, what Eq. (1) or (2) describes is a boundary value problem that depends on the values of  $\varrho_i(z_0)$ , in which  $z_0$  is the reference height, and temperature only plays a role through the equations of state. Therefore, the resulting abundances at certain heights may differ by orders of magnitude from atmospheric models that holistically combine the contributions of necessary physical mechanisms (Vernazza et al. 1981; Fontenla et al. 1993; Avrett & Loeser 2008). Such differences then change plasma properties and thus the results from numerical models (Zhang et al. 2021). Moreover, as the resulting stratified plasma is largely not in ionization equilibrium, which directly relates to the local temperature, static atmospheric models given by Eq. (2) cannot be used to start simulations with ionization and recombination, which will drastically change the energy balance. Using Eq. (2) also implies the assumption that collisional interactions between different fluids do not affect the static equilibrium. Intuitively, however, one may still expect collisional interactions between fluids, although such interactions may not always be sufficient to fully couple all fluids (Hansteen et al. 1997). Therefore, it is necessary to revise the assumption of independent hydrostatic equilibria for different fluids.

Obtaining an initial atmospheric model that is not only in hydrostatic equilibrium but also in ionization equilibrium, thus far, is not trivial, and only a few two-fluid low solar atmospheric models have considered both equilibria (Maneva et al. 2017; Zhang et al. 2021; Niedziela et al. 2024; Kraśkiewicz & Mursawski 2025). Indeed, it is possible to run a long(er) physical-time simulation to reach a steady state (Brchnelova et al. 2023), in which the initial imbalances disappear. However, the numerical solution depends on the chosen initial conditions, and it is difficult to constrain the solution to obtain a specific atmospheric composition. It can also be computationally intensive. Therefore, to obtain an initial static stratification for a multi-fluid-multi-species (MFMS) MHD model that may include various heavier elements (Wargnier et al. 2023; Martínez-Sykora et al. 2023) in addition to hydrogen, an alternative solution is needed.

To construct an MFMS hydrostatic equilibrium atmospheric model, we assume a static configuration in the absence of external disturbances or force imbalances, such that the characteristic timescale of the equilibrium state is infinitely larger than the collisional timescales. Therefore, we may assume that all the  $n$  fluids are coupled by collisional interactions or other mixing processes<sup>1</sup>, approximately acting as a single fluid (Khomenko &

Collados 2012; Martínez-Sykora et al. 2012) in the static state. Then, the gravitational stratification can be calculated straightforwardly. Zhang et al. (2021) used this idea to provide initial equilibria for pure-hydrogen two-fluid plasmas under an isothermal condition. The idea can be extended to MFMS modeling by using a simple numerical integration routine, which is the focus of this work. Below, we start to explain this simple idea with an isothermal example similar to those of Zhang et al. (2021), and then more realistic temperature stratification and ionization are taken into account. We also address the essential physical and numerical consequences of using our model. Additional details are introduced in the Appendix.

## 2. An isothermal example

To explain the idea of this work and its necessity, we extend the solution given by Zhang et al. (2021). We further include neutral and ionized helium ( $\text{He}$  and  $\text{He}^+$ ), in addition to the neutral and ionized hydrogen ( $\text{H}$  and  $\text{H}^+$ ), and thus the model has two species and four fluids (not counting free electrons). Extending the solution to more species and fluids is straightforward and will be discussed later.

We assume an upper chromospheric condition adopted from a 2.5D radiative MHD (rMHD) model (Martínez-Sykora et al. 2020a) using the *Bifrost* code (Gudiksen et al. 2011). The condition was found in regions where the ponderomotive force may produce chemical fractionation, associated with spicules or low-lying loops (Martínez-Sykora et al. 2023). Specifically, the temperature considered is  $1.6 \times 10^4$  K, and the number densities of  $\text{H}$ ,  $\text{H}^+$ ,  $\text{He}$ , and  $\text{He}^+$  were found to be respectively  $10^{9.8}$ ,  $10^{10.7}$ ,  $10^{9.7}$ , and  $10^{8.3}$  per  $\text{cm}^3$ . These number densities are a result of solving for nonequilibrium ionization (NEQ), i.e. solving the full time dependent rate equations for hydrogen and helium. Note that when instead the rMHD model assumes statistical equilibrium (SE) ionization, i.e. solving the rate equations without any  $\partial N_i / \partial t$  term, where  $N_i$  is the number density of the  $i$ -th fluid, the composition includes significantly more neutral fluid. However, in the present example, changing ionization fractions does not affect the conclusions drawn in this paper.

In the original MFMS modeling, gravitational stratification was not considered (Martínez-Sykora et al. 2023). Here, as a first step to improve the MFMS model, we calculate and discuss two different types of stratification:

- (I) Pure hydrostatic equilibrium (pHE): Each fluid is treated independently and satisfies its own hydrostatic equilibrium condition, as given by Eq. 2.
- (II) Coupled hydrostatic equilibrium (cHE): The hydrostatic equilibrium is established through the coupling between different fluids, such that their equilibrium states are mutually dependent.

As constructing the pHE is straightforward, we only introduce the cHE in detail.

As we assume that in the cHE stratification all fluids are coupled by collisional interactions, at each height all fluids can be described by their bulk motion. Therefore, we define an equivalent atomic mass for considering the bulk motion, which reads

$$\bar{m}_T = \frac{\sum_{i=1}^{n+1} N_i m_i}{\sum_{i=1}^{n+1} N_i}, \quad (5)$$

<sup>1</sup> This assumption is, however, not valid higher up in the solar atmosphere and the solar wind, where the plasma gradually becomes collisionless and different fluids/species become decoupled (Hansteen et al. 1994; Hansteen & Leer 1995). The present MFMS model is expected to be used for the low solar atmosphere.

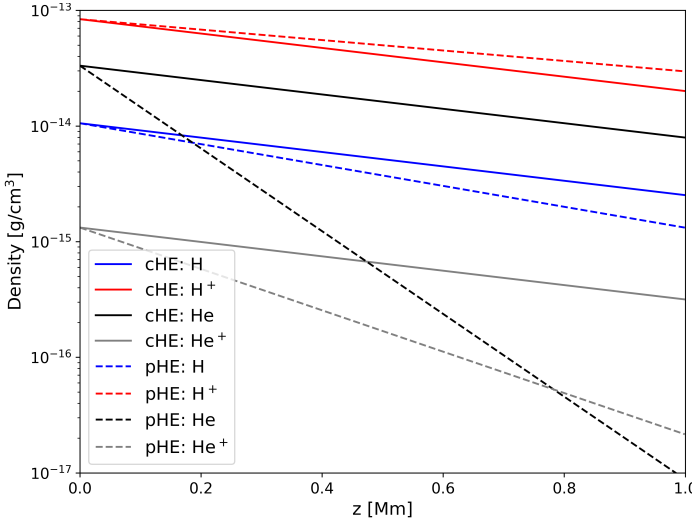


**Fig. 1.** Density stratifications of hydrogen-helium isothermal mixtures. The solid lines are the cHE stratification and the dashed lines are the pHE stratification, both having the same ionization fractions at the reference height ( $z = 0$  Mm).

where  $m_i$  is the atomic mass of the  $i$ -th fluid. Importantly, free electrons should be considered (thus the  $n+1$ -th fluid) when calculating the equivalent atomic mass, while the electron mass is assumed to be zero. As has been mentioned, in this example we have four "non-zero-density" fluids and thus  $n = 4$ . Note that we do include separate equations to describe the motion of electrons, as further explained in Section 4. While assuming the ideal gas law, we have the equation of state written as

$$p_T^g = N_T k_B T, \quad (6)$$

where  $p_T^g$  is the plasma total thermal pressure,  $N_T = \sum_{i=1}^{n+1} N_i$ . Finally, Eq. (1) can be rewritten for the MFMS model, giving us

$$\frac{dP}{dz} = -N_T \bar{m}_T g = -\frac{p_T^g \bar{m}_T g}{k_B T}. \quad (7)$$

For the non-magnetic and isothermal case we discuss in this section, an analytical solution

$$p_T^g = p_{T,z=0}^g \exp\left(-\frac{\bar{m}_T g z}{k_B T}\right), \quad (8)$$

is easily obtained.

In Figure 1, we compare the pHE and cHE results given within a 1 Mm interval<sup>2</sup>, using the aforementioned NEQ number densities to provide the plasma quantities at  $z = 0$ , with a constant temperature  $1.6 \times 10^4$  K. The pHE solution results in exponentially changing ionization fractions, especially for neutral helium, whose atomic mass is the largest and requires a larger pressure gradient to balance. In contrast, the cHE solution maintains close to constant ionization fractions for all fluids, which should be the case when the temperature is constant and plasma dynamics are not yet involved. In the cHE solution, each fluid is not in pure hydrostatic balance. Instead, gravity is balanced by the combination of the pressure gradient and the collisional

forces, assuming that collisions are sufficiently strong. Therefore, in a cHE stratification the velocity of each fluid is not zero, but their total velocity ( $w_T$ ) along the  $z$  direction

$$w_T = \frac{\sum_{i=1}^n \varrho_i w_i}{\sum_{i=1}^n \varrho_i}, \quad (9)$$

is approximately zero. A similar formula is introduced by Khomenko et al. (2014) for the velocity of the center of mass in the one-fluid model, which also explains the static assumption we use before any dynamic driving force is imposed. However, we do not include electrons when defining the total velocity, as the electron velocity is defined as a function of velocities of ions and the total current, i.e. Eq. (13).

Given that ionization fractions affect wave propagation, it is incorrect to use pHE to compute gravitational stratification, except in regions where collisional interactions and other mixing processes are negligible (Hansteen et al. 1997), resulting in decoupled fluids. Moreover, using pHE leads to a higher total density of all fluids, changing wave speeds, etc., thus affecting wave propagation and damping (Zhang et al. 2021). More specifically, the logarithmic slope is different for each of the fluids in pHE vs. cHE. We should also mention that in this simple example the difference in the density distributions of the same fluid in pHE and cHE can already be orders of magnitude. This kind of difference will become more significant when heavier species that have different pressure scale heights are included, and thus it is effectively inviable to use the pHE stratification in MFMS models for evaluating, e.g., the so-called FIP (first ionization potential) effect. Overall, this example shows that it is crucial to construct cHE conditions with physical mixing processes, including, but not limited to, collisional interactions (Hansteen et al. 1994, 1997), particularly for MFMS modeling.

### 3. General scenarios

The previous section shows that MFMS plasma can be in a static equilibrium resulting from the balance between gravity, pressure gradients, and collisional forces between fluids. In an isothermal environment, Eq. (7) is easily solved using an analytical solution. In more general scenarios, in which temperature is not constant, ionization fractions should vary accordingly. Therefore, a numerical integration routine is needed.

Below, we assume that the ionization fractions of all species are already given over the entire 1D domain and are not constant. The ionization fractions can be given by assuming the SE condition under realistic solar atmospheric temperature distributions, or provided by self-consistent rMHD simulations. We numerically discretize Eq. (7) to

$$\frac{\Delta P_j}{\Delta z_j} = \frac{\Delta p_{T,j}^g + \Delta p_j^m}{\Delta z_j} = -\frac{p_{T,j}^g \bar{m}_{T,j} g_j}{k_B T_j}, \quad (10)$$

where the magnetic pressure is given independently. Then we may rewrite Eq. (10) into an integration formula

$$P_{j+1} = P_j - \frac{p_{T,j}^g \bar{m}_{T,j} g_j}{k_B T_j} \Delta z_j, \quad j = 0, \dots, M, \quad (11)$$

where  $M$  is the number of intervals used to calculate the stratification, and  $\bar{m}_{T,j}$  and  $T_j$  are respectively calculated using Eqs. (5) and (6).  $M$  is preferably larger than the number of grid points used in numerical simulations, to reduce the error in the obtained stratification. This is beneficial as the current integration routine

<sup>2</sup> This interval is not suggested to be a realistic layer of the solar atmosphere.

is effectively a first-order left Riemann sum, and it can be applied to either a constant or varying  $\Delta z$ . The present solution is intuitively straightforward, as each integration step is an isothermal scenario introduced in the last section. However, the assumptions we use also imply that neither the hydrostatic equilibrium nor the ionization equilibrium is strictly maintained between any pair of neighboring numerical grid points, thus meaning that a cHE stratification is only in equilibria approximately. Moreover, while collisional interactions are needed to balance gravity and pressure gradient, there must be drift velocities between fluids. Only the total velocity of all fluids is expected to be approximately zero, as has been mentioned above. More details on the remnant disturbances due to the numerical error and the physical decoupling (drift velocities) between fluids are explained in Section 5.

### 3.1. Revisiting the SE assumption

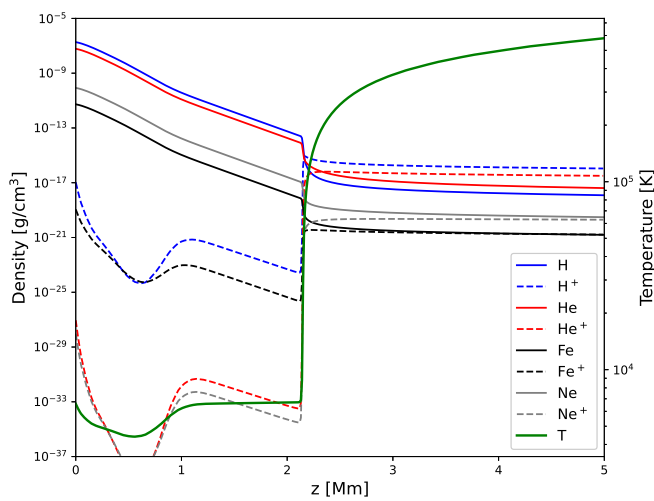


**Fig. 2.** The cHE stratification of a hydrogen-helium-iron-neon mixture under the Model C7 temperature distribution.

We calculate an SE stratification by first extracting the temperature distribution from the widely used Model C7 of Avrett & Loeser (2008). The total number density at the bottom of the photosphere ( $z = 0$  Mm) is approximated using the hydrogen number density given by Model C7, as ion and electron number densities are still small on the solar surface. In addition to the four fluids included in Section 2, we further include Ne,  $\text{Ne}^+$ , Fe, and  $\text{Fe}^+$ . Then, SE ionization under the given temperature distribution is calculated to provide the number densities of these eight fluids, using the ionization and recombination rates of Voronov (1997) and McWhirter (1965), with photospheric abundances of Asplund et al. (2021) provided through the CHIANTI atomic database, Version 11.0 (Dufresne et al. 2024). Note that we calculate only the cHE distributions here, because pHE would lead to significant deviations in the resulting ionization fractions, as explained in the previous section. The cHE stratification is shown in Figure 2.

We find that the total ion density below the transition region (TR) is around 10 orders of magnitude lower than the total neutral density, which relates to several factors. Firstly, the ionization state of hydrogen and helium is computed in SE including collisional ionization balanced by radiative and three

body recombinations (for heavier ions dielectronic recombinations would also be included), using rates from the CHIANTI package (Del Zanna & Mason 2018), while leaving out photoionizations. In addition, as mentioned, SE may underestimate ion fractions due to slow ionization and recombination rates for some transitions. Thus, in the upper chromosphere, NEQ ionization is required, while in the photosphere, solving the Saha equation (Saha 1920) including all species is needed, as metals with their low FIP are the main donors of electrons. A more realistic calculation of SE ionization was presented by Gómez-Míguez et al. (2024), who used the MULTI code (Carlsson 1986) to solve the radiative transfer equation together with the rate equations thus including photoionization correctly. However, calculating the ionization fractions is not the goal of this work, and Figure 2 shows that, most importantly, over the whole domain, at each height, the ionization fractions are in SE. Therefore, the present cHE stratification is very close to both hydrostatic equilibrium and SE. In the following, we further show that a cHE stratification can be constructed for more complicated settings.

Moreover, one may observe that within the temperature plateau of the chromosphere, the ionization fractions stay stable, suggesting that, without considering more realistic chromospheric dynamics, SE ionization cannot produce the increasing trend of ionization fractions in the upper chromosphere.

### 3.2. cHE stratification in NEQ

The previous stratification is given directly using the ionization and recombination rates in SE, but the ionization fractions of different species can be extracted from, e.g., Bifrost simulations. Here we prove the flexibility of the present numerical integration routine, which is applicable as long as temperature and ionization fraction distributions are provided.

We adopt a NEQ simulation snapshot from the 2.5D rMHD model Martínez-Sykora et al. (2020a), as shown in Figure 3. In this model, we observe  $\sim 50$  Mm long loops, which are associated with the underlying magnetic field configuration, which has two main opposite polarities. Correspondingly, there are cold and dense features with chromospheric temperature along the loops, resembling spicules and jets (Martínez-Sykora et al. 2017). More details of the rMHD simulation are, however, not further discussed here. We calculate the horizontally-averaged density and temperature, and then again use the method introduced in Section 3.1 to obtain the SE ionization fractions. Note that the result here includes two-times ionized helium ( $\text{He}^{2+}$ ) but not iron or neon, resulting in a two-species-five-fluid mixture. For comparison, we also extract the averaged ionization fractions directly from the 2.5D snapshot, replacing the SE ionization fractions, to perform the same integration routine. We obtain two stratifications shown in Figure 4, while omitting the contribution of magnetic pressure gradient. The inclusion of magnetic pressure is briefly discussed in Appendix A. Note that both stratifications are calculated using the same temperature distribution.

Due to the horizontal averaging, we obtain a relatively flat TR from the rMHD model. Still, the aim is to show that a cHE stratification can be obtained to include effects of NEQ ionization. Specifically, the NEQ stratification has higher ion populations in the chromosphere and photosphere. Note that the high ion fractions in the NEQ result are related to the long time-scales of the ionization and recombination processes, as well as their interplay with chromospheric dynamics, e.g., shocks (Carlsson & Stein 1992, 2002; Leenaarts et al. 2007; Wedemeyer-Böhm & Carlsson 2011). Therefore, the present numerical integration routine provides flexibility for specifically studying atmospheric

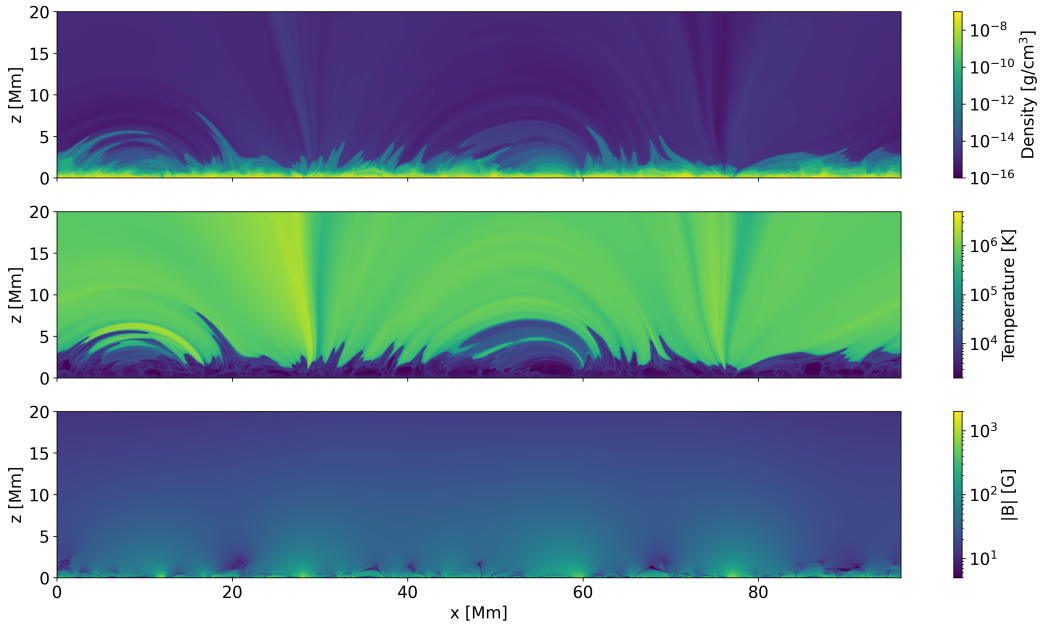


**Fig. 3.** A snapshot of a rMHD simulation with NEQ ionization. Top: density; middle: temperature; bottom: magnetic field strength. Loops and spicules are observed in the snapshot. These structures are dynamic but also relatively steady compared to, e.g., high-frequency waves that may be responsible for local heating or the FIP effect.

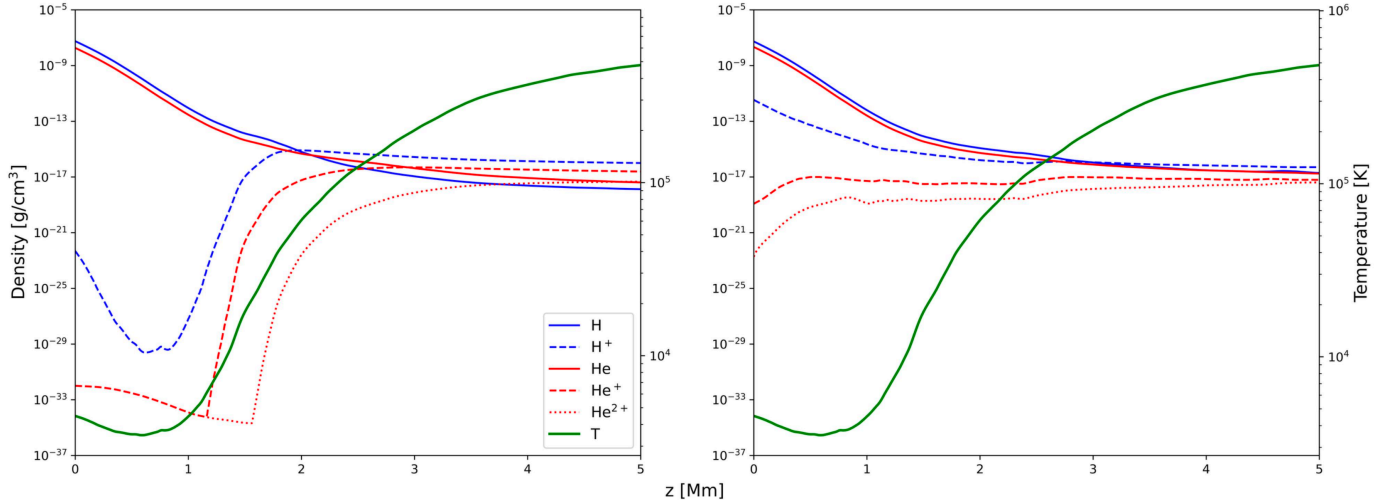


**Fig. 4.** Two cHE stratifications calculated based on the rMHD simulation snapshot. Left: ionization fractions are calculated assuming SE and using the averaged total density and temperature from the rMHD model; right: NEQ ionization fractions are directly given as the averaged ionization fractions from the rMHD model. A small value is used as the floor when calculating ionization fractions in SE, which is a practical treatment for simulations but serves here only for the convenience of visualization, without affecting our conclusions.

dynamics while considering the NEQ ionization effects. In contrast, a pHE stratification cannot recover such effects, as shown in Figure 1.

#### 4. MFMS equations and numerical methods

In the following, we run 1D MFMS numerical simulations that use the stratifications considered above as initial conditions. We use the numerical code **Ebysus** (Martínez-Sykora et al. 2020b, 2023; Wagnier et al. 2023, 2025). Compared to various multi-fluid codes (Alvarez Laguna et al. 2016; Popescu Braileanu et al. 2019; Popescu Braileanu & Keppens 2022; Snow et al. 2023), an

important feature of **Ebysus** is that it can solve the MHD equations separately for each of the desired number of excited levels, ionization stages and species, although in this work, we solve the collective motion of all the excited levels of each neutral species for simplicity. **Ebysus** is modular and allows for the inclusion of ionization/excitation in NEQ, collision between different fluids, thermal conduction, radiative losses, and the Hall term. Details of the derivation of the MFMS formulae have been introduced by Khomenko et al. (2014); Ballester et al. (2018). For the purpose of this work, we neglect the Hall term and thermal conduction as well as considering only 1D as detailed in the next two sections.

In Ebysus, the momentum equation of electrons is used to calculate the electric field, ignoring the inertia of the electrons and their time variation. The electron number density is not an independent variable but is determined by the number densities and ionization states of all the ions, i.e.

$$N_e = \sum_{al} N_{al} Z_{al}, \quad (12)$$

where  $Z$  is the ionized state,  $a$  indicates the identity of the chemical species, and  $I$  denotes the ionization states, with  $I = 0$  denoting neutrals and  $I > 0$  ions. In addition, as the quasi-neutrality approximation is assumed, the electron velocity is expressed as a function of the hydrodynamic velocities of ions and the total current  $\mathbf{J} = \nabla \times \mathbf{B}/\mu_0$ , i.e.

$$\mathbf{u}_e = \sum_{al} \frac{N_{al} q_{al} \mathbf{u}_{al}}{N_e q_e} - \frac{\mathbf{J}}{N_e q_e}, \quad (13)$$

where  $q_{al}$  is the ion charge. Note that, while considering fewer species, similar formulae were also used by Martínez-Gómez et al. (2016).

More importantly, Ebysus solves a separated energy equation of electrons along with the energy equations of ions and neutral fluids. Consequently, the contribution of electron pressure (gradient) is not directly included in the momentum and energy equations of ions. Whereas, the electron pressure contributes to the electric field, which is then included in the momentum equations of ions. Thus, electron pressure also contributes to the induction equation, which reads

$$\frac{d\mathbf{B}}{dt} = \nabla \times \mathbf{E} = \nabla \times \left( \mathbf{u}_e \times \mathbf{B} - \frac{\nabla p_e}{N_e q_e} - \frac{\sum_{al} \mathbf{R}_e^{eal}}{N_e q_e} \right), \quad (14)$$

where  $\mathbf{R}_e^{eal}$  denotes the collisional interactions between electrons and other fluids. Therefore, the electron pressure gradient (thus the Biermann battery term, i.e., the second term on the right-hand side of Eq. (14)) is necessary for Ebysus to account for the contribution of electron pressure in gravitationally stratified atmospheric models.

To spatially discretize the governing equations, Ebysus uses a sixth-order finite-difference scheme with hyper-diffusivity. Fifth-order interpolation is used to interpolate variables in the staggered grid system. To advance in time, we use the modified explicit third-order predictor-corrector Hyman method (Hyman 1979). These numerical approaches are inherited from the **Bifrost** code (Gudiksen et al. 2011). Recently, we have included in Ebysus the second-order Partitioned Implicit-Explicit Orthogonal Runge-Kutta (PIROCK) method (Abdulle & Vilmart 2013; Wargnier et al. 2025), allowing for advancing in time by combining efficient explicit stabilized and implicit integration techniques while employing variable time-stepping with error control. PIROCK method is also tested in this work, further supporting the present results.

## 5. Remnant disturbances and static decoupling

### 5.1. Initial conditions

A cHE stratification obtained using the numerical integration routine is approximately in equilibrium. Therefore, there will be remnant disturbances when a simulation uses the cHE stratification as the initial condition. More importantly, according to our assumption, there must be drift velocities between fluids, which are related to the total pressure gradient in the model. To evaluate these effects, we simulate disturbances developing

in initially quiet stratifications, without imposing any external dynamic driving force. Specifically, we construct a cHE stratification using the Model C7 temperature distribution, yet including only<sup>3</sup> 2.2 to 3.2 Mm and hydrogen and helium (no  $\text{He}^{2+}$ ). Therefore, the domain does not include the non-smooth transition from the upper chromosphere to the TR at around 2.14 Mm in the Model C7. We include only the smooth (yet steep) variation above the transition, where pressure gradient is large.

The resulting initial cHE stratification (Figure 5, left panel in solid lines) is similar to the result shown in Figure 2 for the selected domain. The corresponding simulation result at 0.5 s (Figure 5, left panel in dashed lines) is also shown, and is discussed later. Across the whole domain of the cHE stratification, plasma is approximately in SE, and thus higher up in the domain the helium ionization fraction continues to increase with increasing temperature. Correspondingly, the fractions of neutrals gradually decrease. For comparison, the initial pHE stratification constructed using the same plasma conditions at  $z = 2.2$  Mm as the cHE stratification is shown with solid lines in Figure 5, right panel. In the initial pHE stratification, the ionization fractions do not change with the (rapidly) increasing temperature, and thus the plasma is not in SE.

The initial condition is imposed on 500 evenly distributed grid points that discretize the domain. The mesh is sufficiently fine for the present simulations, and thus we can avoid the effect of numerical diffusion.

### 5.2. SE evolution

Using the given initial conditions we run simulations without any additional dynamic driving force. The simulations use physically calculated collisional frequencies (Wargnier et al. 2022), and include the NEQ ionization and recombination processes. We compare the temporal variations of densities in the simulation using the cHE stratification as the initial condition, as shown with dashed lines in Figure 5, left panel. The density distributions change little over the simulated time, except near the lower boundary, where more accurate spatial discretization is usually needed (Krause 2019; Wei et al. 2023). Therefore, we may claim that the initial condition is sufficiently close to SE in the whole domain. However, the simulation starting with the pHE stratification develops numerical instability as a result of the rapid ionization caused by the initial nonequilibrium, and thus the corresponding result is not further discussed.

Although the total velocity in the cHE + NEQ simulation is not exactly zero, only small disturbances slowly develop over time, mainly in the lower part of the domain (Figure 6). The decoupling in the cHE result causes collisional forces. In the meantime, the ionization and recombination processes exchange momentum between ions and neutrals, reducing the decoupling. Without ionization and recombination, the decoupling increases over time at a faster rate, until the collisional forces are able to balance the gravity and the pressure gradient, in which case the maximum decoupling between the neutral helium and the total velocity reaches above  $2 \text{ km s}^{-1}$  (not shown). The drift velocities that occur in the cHE stratification are physically important.

<sup>3</sup> The Model C7 provides discrete data points. Therefore, the temperature distribution is interpolated using the `interp1d` function from the `NumPy` library (Harris et al. 2020) with the `quadratic` interpolation method. While errors still exist, using the `linear` method would have caused more significant errors in drift velocities and, eventually, in the total velocity. The error in the interpolated temperature distribution is not observable by the naked eye, but it affects the sound speed and pressure gradient.

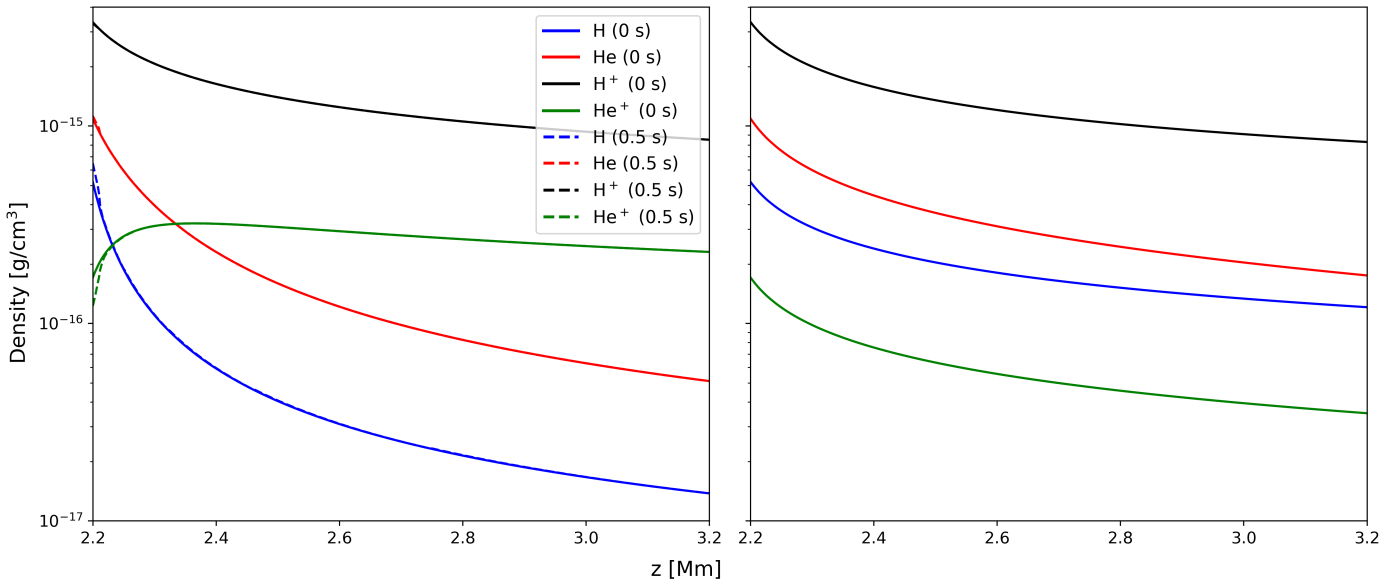


**Fig. 5.** Left: density distributions at  $t = 0$  s and  $t = 0.5$  s when using the cHE stratification as the initial condition for a simulation with NEQ ionization/recombination, but without any dynamic driving force; right: the pHE stratification (viz. at  $t = 0$  s). Using the pHE stratification as the initial condition leads to numerical instability in simulations with ionization/recombination, and thus the results are not included.

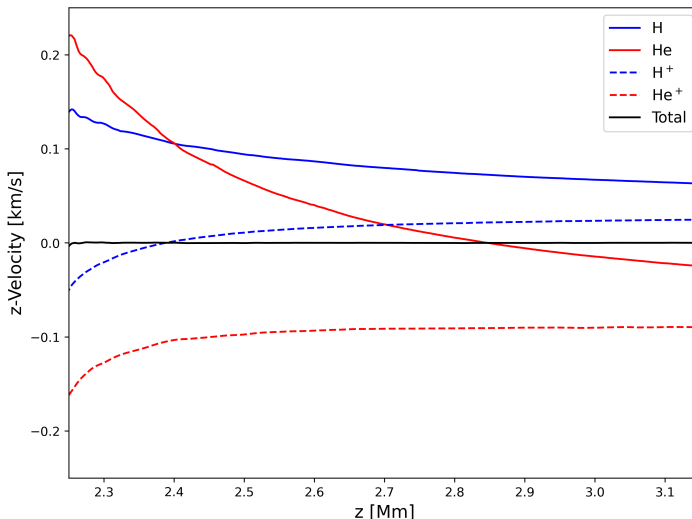


**Fig. 6.** Longitudinal velocities of the cHE + NEQ simulation shown in Figure 5 at  $t \approx 0.5$  s. The total velocity and the velocities of all fluids are shown. Initial velocities are all zero.

In particular, such drift velocities are an important difference between single-fluid and multi-fluid models (Gómez-Míguez et al. 2025).

The results suggest that the pHE stratification is not viable for simulations that include ionization and recombination, as numerical instability may occur. Even if ionization and recombination are not activated, the ionization fractions are important for correctly describing the collisional interactions. For example, in Figure 5, the density of the neutral hydrogen in the pHE stratification can be around an order of magnitude higher than that of the neutral hydrogen in the cHE stratification, and this difference certainly affects collisional frequencies.

Moreover, the cHE model provides a steady solution with chemical fractionation for a gravitational settling of the solar atmosphere, accounting for the effects of ionization and recombi-

nation. Note that in the solar atmosphere, dynamic phenomena such as MHD waves may also be responsible for chemical fractionation (Laming 2004, 2015), and the present cHE stratification can be used to numerically model the dynamic effects.

## 6. The ponderomotive force and the resulting motions

Since significant decoupling appears in the cHE stratification when the pressure gradient is large, it is interesting to know how this "static" decoupling would contribute to the MFMS dynamics. Here, we run simulations of a monochromatic Alfvén wave, using the cHE and pHE stratifications introduced in the previous section. Alfvén waves existing in the low solar atmosphere have been suggested (De Pontieu et al. 2007; McIntosh et al. 2011; Chae et al. 2021), and they may play a vital role in coronal heating (Van Doorsselaere et al. 2020), the FIP effect (Laming 2004, 2015), etc., which are beyond the scope of this work. We are interested in the fact that the ponderomotive force caused by Alfvén waves drives plasma motions along the magnetic field, and such motions can be simulated and used as an example to compare the effects of using different stratifications.

An initially constant vertical magnetic field  $B_z = 10$  G is imposed on the stratifications discussed in the previous section, and the Alfvén wave is driven by periodically changing  $B_x$  at  $z = 2.2$  Mm, similar to what was done by (Martínez-Sykora et al. 2023). Note that such a driver may not be suitable in the weakly ionized photosphere (Cally 2023), but works under the present atmospheric condition. The frequency of the driver is 1 Hz, and the amplitude is 1 G. The resulting amplitude of the velocity along the  $x$  direction is  $\sim 40$  km s $^{-1}$ . Based on this basic setting, five simulations are performed, as listed in Table 1. We mainly focus on comparing the differences between using cHE and pHE stratifications, with or without the NEQ ionization (simulations (c)-(e)). Because of the numerical instability mentioned in the previous section, the pHE stratification is only discussed without including ionization and recombination in the simulation (simulation (d)). We also include two simulations that use non-physical

collisional frequencies to examine the weakly and strongly collisional scenarios (simulations (a) & (b)). These two non-physical frequencies are, respectively, significantly lower and higher than the imposed wave frequency. The former should evolve as separated fluids and the latter should recover the single fluid scenario.

**Table 1.** Summary of the simulations.

	Stratification	Ionization	Collisional Frequency
(a)	cHE	–	0.05 Hz
(b)	cHE	–	100 Hz
(c)	cHE	–	physical
(d)	pHE	–	physical
(e)	cHE	NEQ	physical

The effects of the numerical disturbances appear mainly in the  $z$  direction (i.e., the direction of the magnetic field). Moreover, the Alfvén wave induces ponderomotive force, driving plasma motions along the magnetic field. Therefore, the longitudinal velocity components are compared in Figure 7. Apparently, when it is weakly collisional (panel a), the neutral fluids are decoupled from the ionized fluids, whose motions are driven by the Alfvén wave. Each neutral fluid also moves independently because of the imbalance between gravity and the respective plasma gas pressure, while neither collisions with ionized fluids nor magnetic pressure affect neutral fluids. In contrast, all fluids in the strongly collisional simulation are coupled, behaving as a single-fluid as expected (panel b). More importantly, we can observe that in the strongly collisional simulation, the total velocity is zero before the wave arrives, showing that the cHE stratification is indeed in hydrostatic equilibrium, providing another way to validate the MFMS code – once it is collisionally coupled the plasma behaves as a single fluids.

Simulations using physical collisional frequencies (Wargnier et al. 2022) show significant decoupling of neutral helium (panels c-e). A similar result was also obtained by Martínez-Gómez et al. (2018), although only initially homogeneous media were considered. Wargnier et al. (2023) also found that neutral helium is more significantly decoupled from other fluids during upper-chromospheric magnetic reconnection. Thus, including helium may be important for modeling the dynamics across the TR. Moreover, when using cHE stratification (panels c and e), neutral helium has a higher longitudinal velocity than pHE (panel d), due to the contribution of the pressure gradient, which is more obvious in Figure 6. The ionization process strengthens the interactions between ionized and neutral fluids, thereby increasing the coupling in the simulation (e). Nevertheless, in general, neutral helium has smaller longitudinal velocity than the other fluids.

The pHE stratification is not further discussed with ionization and recombination due to the numerical instability. We should however note that, the ionization and recombination timescales are long in the chromosphere (Carlsson & Stein 2002), and thus the changes in density and temperature would be less drastic when the pHE stratification is used under chromospheric conditions. However, this also means that the ionization fractions (and thus the collisional interactions) in the corresponding simulations would be largely dependent on the initial stratification. We have shown in Section 2, that heavier elements, whose scale heights are different from that of (ionized or neutral) hydrogen, cannot be properly recovered by the pHE stratification, even if the collisional interactions (or other mixing processes) are sufficient to couple the heavy fluids.

## 7. Conclusions and outlook

The primary goal of this work is to provide gravitationally stratified initial/background fields for MFMS modeling. This goal is achieved using a simple numerical integration routine based on relaxed equilibrium assumptions. Specifically, as an initial static condition is given, we may assume that all fluids can be coupled by the collisional interactions, which may then contribute to the hydrostatic equilibrium (viz. the cHE stratification) and allow us to account for any expected ionization fractions, especially including the SE ionization fractions. Without such initial fields, it is difficult to include both gravitational stratification and ionization/recombination simultaneously, since instability or disturbances caused by initial inequilibria in the pHE stratification can lead to significant errors and even sabotage numerical modeling. The present work is even more critical when more species are needed, whose pressure scale heights are vastly different, in which case the purely hydrostatic stratification (viz. the pHE stratification) is far from being in ionization equilibrium and heavy elements effectively disappear. More specifically, the cHE stratification provides a gravitational settling for chemical fractionation, in which heavy elements are (partly) supported by collisional interactions, with no other dynamic driving mechanisms included.

The present cHE stratification also clearly shows the drift velocities accompanied by strong pressure gradients, which are more prominent in the TR. Such drift velocities (decoupling between fluids) are deemed physical, as the pressure scale heights of different fluids are more significantly different in this region. In contrast, the pHE stratification does not recover such effects, regardless of the pressure gradients, and thus there is no collisional interaction between fluids, which is a strong hypothesis.

Eventually, the present cHE provides a gravitationally stratified "static" atmospheric model that can be used to more specifically and accurately study waves, reconnection, etc., potentially further improving previous MFMS models (Martínez-Gómez et al. 2016, 2017, 2018; Martínez-Sykora et al. 2020b; Wargnier et al. 2023; Martínez-Sykora et al. 2023). Note that multi-fluid effects have been discussed with regard to various topics, and including (only) hydrogen and helium suffices in many cases. However, numerical models of the FIP effect, particularly, need to explicitly include heavier elements, which has been challenging. The present work shows that, for example, the ponderomotive force and the resulting motions can be modeled using the cHE stratification, which allows gravitational stratification and NEQ ionization to be incorporated into the previously semi-homogeneous MFMS model (Martínez-Sykora et al. 2023).

In addition, we have artificially increased (or decreased) the collision rate producing a strongly (or weakly) coupled models behaving as single fluid (or independent fluids). This parametric study briefly visualizes the importance of properly describing the interactions between fluids, which may substantially change the properties of the plasma (Hansteen et al. 1997). Moreover, the result also further addresses that Ebysus code is capable when the interactions are sufficient to couple all the fluids and returns single fluid scenario.

In this work, we only discuss (quasi-)1D scenarios, in which case it is easy to account for the contribution of the magnetic field. Similarly, the cHE stratification can be directly used under multi-dimensional force-free magnetic fields. The extension to multi-dimensional non-force-free scenarios is left for future work.

*Acknowledgements.* FZ would like to thank Nicolas Poirier, Mats Carlsson, Ben Snow for the helpful discussion, and Mikolaj Szydlarski for the technical sup-

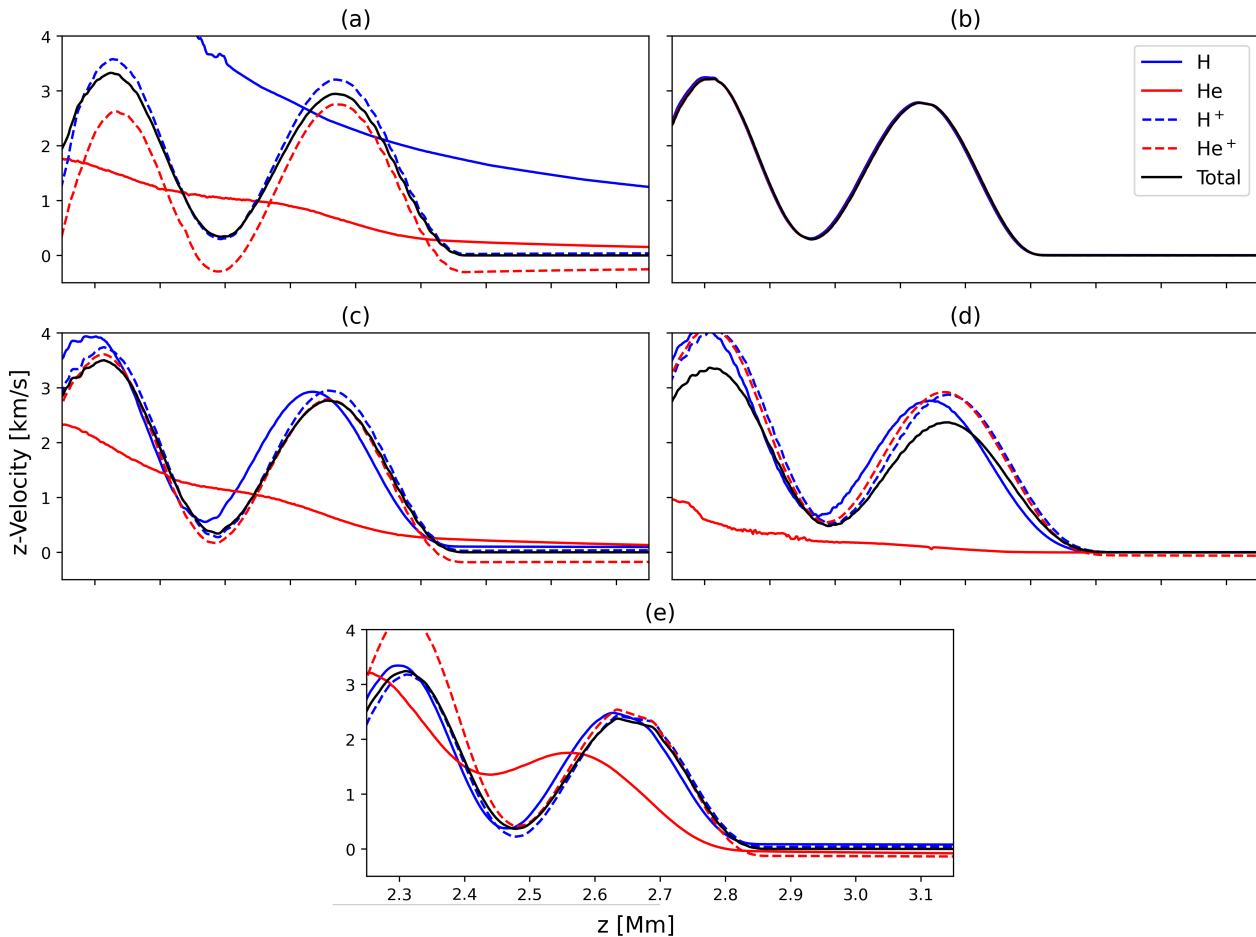


**Fig. 7.** Longitudinal velocities at  $t = 1$  s. All settings are listed in Table 1. Except simulation (d) which uses the pHE stratification, all the others use the cHE stratification as the initial condition. Simulations (a) and (b) use assigned constant collisional frequencies. More specifically, (a) is weakly collisional and (b) is strongly collisional, respectively having collisional frequencies  $5 \times 10^{-2}$  Hz and  $10^2$  Hz. All the other simulations use physical collisional frequencies calculated by Ebysus. Only simulation (e) includes the NEQ ionization/recombination.

This research is supported by the Research Council of Norway through its Centres of Excellence scheme, project number 262622. JMS acknowledges support by NASA contract NNG09FA40C (IRIS) and 80GSFC21C0011 (MUSE), NASA grant 80NSSC26K0018, NSF grants AGS2532363 and AGS2532187. This work used the CHIANTI atomic database. CHIANTI is a collaborative project involving George Mason University, the University of Michigan (USA), the University of Cambridge (UK), and NASA Goddard Space Flight Center (USA). Figures in this work were produced using the python package `Matplotlib` (Hunter 2007). Data processing was performed using the `NumPy` library (Harris et al. 2020) and in-house packages `EbysusRunTools_py`, `atom_py` and `Helita`.

## References

Abdulle, A. & Vilmart, G. 2013, *Journal of Computational Physics*, 242, 869  
 Alvarez Laguna, A., Lani, A., Deconinck, H., Mansour, N., & Poedts, S. 2016, *Journal of Computational Physics*, 318, 252  
 Asplund, M., Amarsi, A. M., & Grevesse, N. 2021, *A&A*, 653, A141  
 Avrett, E. H. & Loeser, R. 2008, *The Astrophysical Journal Supplement Series*, 175, 229  
 Ballester, J. L., Alexeev, I., Collados, M., et al. 2018, *Space Science Reviews*, 214  
 Brchneleva, M., Kužma, B., Zhang, F., Lani, A., & Poedts, S. 2023, *A&A*, 678, A117  
 Cally, P. S. 2023, *The Astrophysical Journal*, 954, 85  
 Carlsson, M. 1986, *Uppsala Astronomical Observatory Reports*, 33  
 Carlsson, M. & Stein, R. F. 1992, *The Astrophysical Journal Letters*, 397, L59  
 Carlsson, M. & Stein, R. F. 2002, *The Astrophysical Journal*, 572, 626  
 Chae, J., Cho, K., Nakariakov, V. M., Cho, K.-S., & Kwon, R.-Y. 2021, *The Astrophysical Journal Letters*, 914, L16  
 De Pontieu, B., McIntosh, S. W., Carlsson, M., et al. 2007, *Science*, 318, 1574  
 Del Zanna, G. & Mason, H. E. 2018, *Living Reviews in Solar Physics*, 15, 5  
 Dufresne, R. P., Del Zanna, G., Young, P. R., et al. 2024, *The Astrophysical Journal*, 974, 71  
 Fontenla, J. M., Avrett, E. H., & Loeser, R. 1993, *The Astrophysical Journal*, 406, 319  
 Gary, G. A. 2001, *Solar Physics*, 203, 71  
 Gómez-Míguez, M. M., Martínez-Gómez, D., Khomenko, E., et al. 2025, *A&A*, 701, A196  
 Gómez-Míguez, M. M., Martínez-Gómez, D., Khomenko, E., & Vitas, N. 2024, *Philosophical Transactions of the Royal Society A*, 382  
 Gudiksen, B. V., Carlsson, M., Hansteen, V. H., et al. 2011, *Astronomy & Astrophysics*, 531, A154  
 Hansteen, V. H. & Leer, E. 1995, *Journal of Geophysical Research: Space Physics*, 100, 21577  
 Hansteen, V. H., Leer, E., & Holzer, T. E. 1994, *The Astrophysical Journal*, 428, 843  
 Hansteen, V. H., Leer, E., & Holzer, T. E. 1997, *The Astrophysical Journal*, 482, 498  
 Harris, C. R., Millman, K. J., van der Walt, S. J., et al. 2020, *Nature*, 585, 357  
 Hunter, J. D. 2007, *Computing in Science & Engineering*, 9, 90  
 Hyman, J. M. 1979, in *Proceedings of the 3rd IMACS International Symposium on Computer Methods for Partial Differential Equations*, Bethlehem, PA, USA  
 Jerčić, V., Popescu Braileanu, B., & Keppens, R. 2025, *The Astrophysical Journal*, 986, 134  
 Karampelas, K., Van Doorsselaere, T., & Guo, M. 2019, *A&A*, 623, A53  
 Khomenko, E. 2016, *Plasma Physics and Controlled Fusion*, 59, 014038  
 Khomenko, E. & Collados, M. 2012, *The Astrophysical Journal*, 747, 87  
 Khomenko, E. & Collados, M. 2015, *Living Reviews in Solar Physics*, 12  
 Khomenko, E., Collados, M., Díaz, A., & Vitas, N. 2014, *Physics of Plasmas*, 21, 092901

Kraśkiewicz, J. & Murawski, K. 2025, A&A, 698, A74

Krause, G. 2019, A&A, 631, A68

Laming, J. M. 2004, The Astrophysical Journal, 614, 1063

Laming, J. M. 2015, Living Reviews in Solar Physics, 12

Leenaarts, J., Carlsson, M., Hansteen, V., & Rutten, R. J. 2007, A&A, 473, 625

Maneva, Y. G., Alvarez Laguna, A., Lani, A., & Poedts, S. 2017, The Astrophysical Journal, 836, 197

Martínez-Gómez, D., Soler, R., & Terradas, J. 2016, The Astrophysical Journal, 832, 101

Martínez-Gómez, D., Soler, R., & Terradas, J. 2017, The Astrophysical Journal, 837, 80

Martínez-Gómez, D., Soler, R., & Terradas, J. 2018, The Astrophysical Journal, 856, 16

Martínez-Sykora, J., De Pontieu, B., & Hansteen, V. 2012, The Astrophysical Journal, 753, 161

Martínez-Sykora, J., De Pontieu, B., Hansteen, V. H., et al. 2023, The Astrophysical Journal, 949, 112

Martínez-Sykora, J., Leenaarts, J., De Pontieu, B., et al. 2020a, The Astrophysical Journal, 889, 95

Martínez-Sykora, J., Szydlarski, M., Hansteen, V. H., & De Pontieu, B. 2020b, The Astrophysical Journal, 900, 101

Martínez-Sykora, J., Pontieu, B. D., Carlsson, M., et al. 2017, The Astrophysical Journal, 847, 36

McIntosh, S. W., Pontieu, B. D., Carlsson, M., et al. 2011, Nature, 475, 477

McWhirter, R. W. P. 1965, in Plasma Diagnostic Techniques, ed. R. H. Huddleston & S. L. Leonard (New York: Academic Press), 201–264

Nakariakov, V. M., Verwichte, E., Berghmans, D., & Robbrecht, E. 2000, A&A, 362, 1151

Niedziela, R., Murawski, K., & Poedts, S. 2024, A&A, 691, A254

Popescu Braileanu, B. & Keppens, R. 2022, A&A, 664, A55

Popescu Braileanu, B. & Keppens, R. 2023, A&A, 678, A66

Popescu Braileanu, B., Lukin, V. S., Khomenko, E., & de Vicente, A. 2019, A&A, 630, A79

Saha, M. N. 1920, The London, Edinburgh, and Dublin Philosophical Magazine and Journal of Science, 40, 472

Snow, B., Druett, M. K., & Hillier, A. 2023, Monthly Notices of the Royal Astronomical Society, 525, 4717

Solanki, S. K., Inhester, B., & Schüssler, M. 2006, Reports on Progress in Physics, 69, 563

Van Doorsselaere, T., Srivastava, A. K., Antolin, P., et al. 2020, Space Science Reviews, 216, 140

Vernazza, J. E., Avrett, E. H., & Loeser, R. 1981, The Astrophysical Journal Supplement Series, 45, 635

Voronov, G. 1997, Atomic Data and Nuclear Data Tables, 65, 1

Wargnier, Q. M., Martínez-Sykora, J., Hansteen, V. H., & De Pontieu, B. 2022, The Astrophysical Journal, 933, 205

Wargnier, Q. M., Martínez-Sykora, J., Hansteen, V. H., & De Pontieu, B. 2023, The Astrophysical Journal, 946, 115

Wargnier, Q. M., Vilmar, G., Martínez-Sykora, J., Hansteen, V. H., & De Pontieu, B. 2025, A&A, 695, A262

Wedemeyer-Böhm, S. & Carlsson, M. 2011, A&A, 528, A1

Wei, Y.-X., Zhang, F., Liu, J., Su, H.-X., & Xu, C.-G. 2023, Computers & Fluids, 252, 105774

Wójcik, D., Kuźma, B., Murawski, K., & Musielak, Z. E. 2020, A&A, 635, A28

Zhang, F., Poedts, S., Lani, A., Kuźma, B., & Murawski, K. 2021, The Astrophysical Journal, 911, 119

## Appendix A: Effects of magnetic field

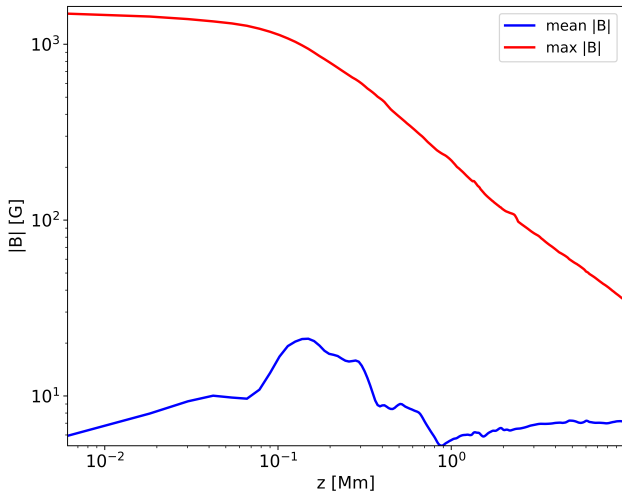


**Fig. A.1.** The maximum and averaged  $|\mathbf{B}|$  at each height. the maximum value shows a clear inverse power law above  $\sim 0.1$  Mm. The averaged value, however, first drastically increases and then gradually decreases, and finally exhibits slow variation above  $\sim 1$  Mm.

The magnetic field is a driving force of the complex dynamics in the solar atmosphere. In particular, locally concentrated magnetic structures in the photosphere may undergo rapid expansion in the low solar atmosphere (Gary 2001; Solanki et al. 2006), resulting in large magnetic pressure gradients that cannot be overlooked when considering gravitational stratification.

Therefore, following the results in Section 3.2, we discuss the effects of adding a magnetic field. The magnetic field in this 2D model is locally concentrated in the photosphere and shows a significant expansion higher up. Consequently, the unsigned mean magnetic field strength decreases over height (Figure 3, bottom). Observing Figure A.1, a power law can be seen from the variation of the maximum value at each height, but it is not representative of the whole magnetic field. The averaged value also cannot represent the derivative (i.e., gradient) of the magnetic field. Nevertheless, we do not intend to focus on such details, and the results justify using an expansion assumption to approximate the effect of magnetic pressure.

Assuming that the (3D) spatial expansion is the only cause reducing the magnetic field strength, we use

$$p^m(z) = 0.5 \left[ \frac{|\mathbf{B}_0|}{(z + r_0)^2 / r_0^2} \right]^2, \quad (\text{A.1})$$

where  $\mathbf{B}_0$  and  $r_0$  are free parameters, to describe the magnetic pressure from the bottom of the photosphere. With Eq. (A.1), a smaller  $r_0$  means that the magnetic field is more concentrated in the photosphere. The pressure gradient can be analytically calculated based on Eq. (A.1), and directly added into the numerical integration routine introduced in Section 3. With a constant  $r_0$  and varying  $\mathbf{B}_0$ , we have obtained a series of stratifications with the SE ionization, as shown in Figure A.2. Note that only the total densities of all fluids are shown for simplicity. We first acknowledge that without magnetic pressure (gradient), the cHE stratification has a lower density than the averaged 2D solution. In comparison, magnetic pressure gradients significantly alter the solution, indicating that stronger gradients support higher

density. More importantly, the results demonstrate that the current numerical integration routine can be used to calculate cHE stratifications under varying magnetic fields.

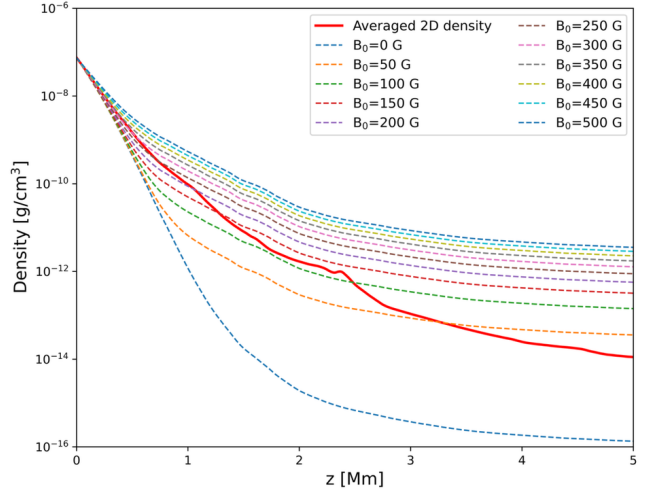


**Fig. A.2.** cHE stratifications calculated with analytical magnetic pressure distributions,  $r_0 = 1$  Mm, and SE ionization fractions. NEQ ionization fractions can also be used to calculate such stratifications. The total density when  $B_0 = 0$  G is the same as the SE result in Figure 4.

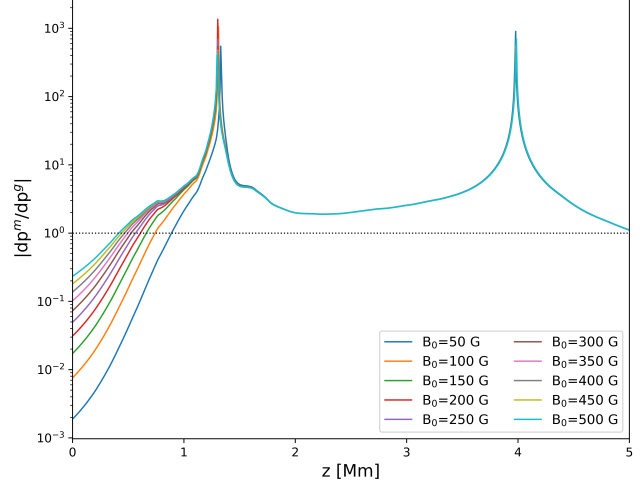


**Fig. A.3.** Ratios of the magnetic pressure gradient to the plasma gas pressure gradient shown in Figure A.2. The peaks appear because the plasma gas pressure gradient changes sign. Above the photosphere, the magnetic pressure gradient becomes dominant in shaping the stratifications.

So far, we have only discussed 1D scenarios with a constant gravitational acceleration. We may also consider stratification along a coronal loop, in which case the gravitational acceleration varies with the loop's curvature. This scenario is relevant for understanding, e.g., wave heating (Karampelas et al. 2019), MHD seismology (Nakariakov et al. 2000), or prominence formation (Jerčić et al. 2025). Without going into the details of realistic magnetic fields, we simply discuss a semicircular loop, for which a cosine function can be used in the integration routine straightforwardly, to revise the balance law between gravity and

pressure gradient, and thus, we have

$$\frac{dP}{dz} = -\frac{p_T^g \bar{m}_T}{k_B T} g \cos\left(\frac{\pi z}{2L}\right), \quad z < L, \quad (\text{A.2})$$

in which  $L$  is the radius of the loop. This function is essentially the same as what was used by Karampelas et al. (2019). As  $z$  is the height from the footpoint, the gravitational acceleration along the loop axis becomes zero at the loop apex ( $z = L$ ). Plasma along a realistic loop is supported by plasma gas pressure and magnetic pressure/tension, and we can already see that the magnetic pressure gradient effectively shapes the 1D stratification. Particularly, Figure A.3 shows that the magnetic pressure description given by Eq. (A.1) results in sufficient magnetic pressure gradients to support the plasma in the upper chromosphere and above, where plasma  $\beta$  is typically smaller than 1. Consequently, including Eq. (A.2) does not significantly change the stratifications, and the corresponding results are not shown for simplicity.

Again, we note that one may directly extract needed variables along open or closed field lines (or other regions of interest) from 2D/3D solar atmospheric models, and cHE stratifications can be constructed based on the extracted variables.